PHYSICAL REVIEW B **91**, 201101(R) (2015)

Engineering the topological surface states in the $(Sb_2)_m$-Sb_2Te_3 ($m = 0$–3) superlattice series

J. C. Johannsen,[1] G. Autès,[2,3] A. Crepaldi,[4] S. Moser,[1] B. Casarin,[4,5] F. Cilento,[4] M. Zacchigna,[6] H. Berger,[1] A. Magrez,[1] Ph. Bugnon,[1] J. Avila,[7] M. C. Asensio,[7] F. Parmigiani,[4,5,8] O. V. Yazyev,[2,3] and M. Grioni[1,*]

[1]*Institute of Condensed Matter Physics, Ecole Polytechnique Fédérale de Lausanne (EPFL), CH-1015 Lausanne, Switzerland*

[2]*Institute of Theoretical Physics, Ecole Polytechnique Fédérale de Lausanne (EPFL), CH-1015 Lausanne, Switzerland*

[3]*National Center for Computational Design and Discovery of Novel Materials MARVEL, Ecole Polytechnique Fédérale de Lausanne (EPFL), CH-1015 Lausanne, Switzerland*

[4]*Elettra-Sincrotrone Trieste S.C.p.A, Strada Statale 14, km 163.5, I-34149 Basovizza, Trieste, Italy*

[5]*Università degli Studi di Trieste, Via A. Valerio 2, I-34127 Trieste, Italy*

[6]*IOM-CNR Laboratorio TASC, Area Science Park, 34149 Trieste, Italy*

[7]*Synchrotron SOLEIL, Saint Aubin, BP 48, F-91192 Gif-sur-Yvette, France*

[8]*International Faculty, University of Köln, D-50937 Köln, Germany*

(Received 7 January 2015; revised manuscript received 24 April 2015; published 11 May 2015)

We investigate the evolution of both the occupied and unoccupied electronic structure in representative compounds of the infinitely adaptive superlattice series $(Sb_2)_m$-Sb_2Te_3 ($m = 0$–3) by means of angle-resolved photoemission spectroscopy and time-delayed two-photon photoemission, combined with first-principles band-structure calculations. We discover that the topological nature of the surface states and their spin texture are robust, with dispersions evolving from linear (Dirac-like) to parabolic (Rashba-like) along the series, as the materials evolve from semiconductors to semimetals. Our findings provide a promising strategy for engineering the topological states with the desired flexibility needed for realizing different quantum phenomena and spintronics applications.

DOI: 10.1103/PhysRevB.91.201101 PACS number(s): 73.20.At, 71.70.Ej, 79.60.−i

Three-dimensional topological insulators (TIs) are materials where the topological properties of the insulating bulk band structure guarantee the existence of metallic surface states [1,2]. These topological surface states (TSS) are characterized by a Dirac-like energy-momentum dispersion and by a helical spin-momentum texture [3,4] that protects them against backscattering and localization [5,6]. TIs are promising materials for spintronics and provide an exceptional playground to study novel physical phenomena [7,8]. Possible applications depend on the ability to control the electronic properties of the TSS. Common strategies for achieving such a control involve chemical substitution and adsorbate doping [9–13]. Alternatively, it has been proposed that multilayer heterostructures could be used to obtain artificial TIs with tunable properties defined by the stacking sequences of the constituent two-dimensional building blocks [14–16].

In this Rapid Communication, we demonstrate the possibility of TSS band-structure engineering in the naturally occurring homologous series of topological superlattices $(Sb_2)_m$-$(Sb_2Te_3)_n$ composed of Sb_2 bilayers (BLs) and Sb_2Te_3 quintuple layers (QLs) [17,18]. This series enables a systematic investigation of the evolution of topological properties as a function of the stacking sequence of the constituent building blocks. Our results show that the topological states are remarkably robust and that their dispersion can be tuned in the explored range ($m = 0$–3; $n = 1$), and in bulk Sb, with an unchanging strong Z_2 index $\nu_0 = 1$.

All $(Sb_2)_m$-$(Sb_2Te_3)_n$ compounds display layered crystal structures produced by ordered stacking of Sb_2Te_3 QLs and antimony BLs along the c axis of the hexagonal unit cell. This provides for an "infinitely adaptive series" of distinct compounds between the end member compositions Sb_2Te_3 ($m = 0$) and Sb ($n = 0$) [17–20] that are known to be a TI and a topological semimetal, respectively [21–27]. Early experiments assessed the topological nature of bulk Sb and Sb-Bi alloys [21,22]. By contrast, the experimental observation of the predicted TSS in Sb_2Te_3 has been delayed by the intrinsic p doping of this material [25,28–30]. The topological properties of the intermediate members of this series still need to be addressed. This motivated angle-resolved photoemission spectroscopy (ARPES) and time-delayed two-photon photoemission (2PPE) measurements [31] of the occupied and unoccupied electronic band structure of two representative compositions Sb_2Te_3 $(m,n) = (0,1)$ and Sb_6Te_3 $(m,n) = (2,1)$, and more systematic first-principles band-structure calculations. The combination of ARPES and 2PPE measurements allows us to track the evolution of both the occupied and unoccupied parts of the band structure of the TSS around the $\bar{\Gamma}$ as the stoichiometry is varied. This provides a k-dependent probe of the unoccupied states, alternative to the experimentally challenging inverse photoemission spectroscopy [32].

High-quality single crystals of Sb_6Te_3 and Sb_2Te_3 were obtained by slowly cooling a molten stoichiometric mixture of high-purity (99.999%) antimony and tellurium in a horizontal furnace and by the vertical variant of the Bridgman technique, respectively. These procedures resulted in silver-colored single crystals of ∼5 mm size. We note here that several other compositions of the $(Sb_2)_m$-$(Sb_2Te_3)_n$ family have been synthesized in crystalline form as small grains [19]. Their microscopic size, however, impedes access to the electronic structure by ARPES. ARPES measurements were carried out at the ANTARES beamline of the SOLEIL synchrotron (St. Aubin) with energy and angle resolution better than 20 meV and 0.15°, respectively. The 2PPE measurements were performed at the T-ReX laboratory (Elettra-Sincrotrone, Trieste) with 25 meV

*marco.grioni@epfl.ch

and 0.3° resolution. All spectra were acquired with linearly *s*-polarized photons. Samples were cleaved in ultrahigh vacuum at ambient temperature and immediately transferred to the measurement position, where they were held at 100 K. The first-principles calculations were performed within the density functional theory (DFT) framework employing the generalized gradient approximation (GGA) as implemented in the QUANTUM ESPRESSO package [33]. Spin-orbit effects were accounted for using fully relativistic norm-conserving pseudopotentials acting on valence electron wave functions represented in the two-component spinor form [34]. For Sb_2Te_3, Sb_6Te_3, and Sb_8Te_3, we used the experimental lattice parameters and atomic coordinates from Refs. [19,35,36]. Since structural data for Sb_4Te_3 are not available, we constructed a model of this compound based on the structure of Bi_4Se_3 [18], and corrected the lattice parameters to match those of the $(Sb_2)_m$-$(Sb_2Te_3)_n$ series. To study the electronic properties of the surface states, we constructed QL-terminated (0001) slab models of Sb_2Te_3, Sb_4Te_3, Sb_6Te_3, and Sb_8Te_3 containing at least 40 atomic layers. The surface state localization and spin texture properties were obtained by projecting the Kohn-Sham wave functions onto atomic orbitals.

Figures 1(a) and 1(d) show the crystal structures of Sb_2Te_3 and Sb_6Te_3, respectively, illustrating the presence of two Sb_2 BLs between QLs in the latter compound [17]. While the covalent bonding within QLs and BLs is strong, the interaction between the neighboring building blocks is of the much weaker van der Waals type [17,18]. As a consequence, the natural cleaving plane in Sb_2Te_3 is located between the QLs and the cleaved surface is always Te terminated. For Sb_6Te_3, three different cleaved surface terminations are possible: Te-rich QL, Sb-rich one-BL, and Sb-rich two-BLs. Here, we consider only the QL-terminated surface, and direct the reader to the Supplemental Material [37] for a discussion of our results for the BL terminations.

The ARPES intensity maps of Figs. 1(b) and 1(e) illustrate the band dispersion of Sb_2Te_3 and Sb_6Te_3, respectively, along the high-symmetry directions $\bar{\Gamma}$-$\bar{M}$ and $\bar{\Gamma}$-$\bar{K}$ of the surface Brillouin zone (SBZ). The main experimental features are well reproduced by the calculated projected band structures for the corresponding QL-terminated slab models in Figs. 1(c) and 1(f). The bulk bands cross the Fermi energy E_F along the $\bar{\Gamma}$-$\bar{M}$ direction for both materials, and also along $\bar{\Gamma}$-$\bar{K}$ in the case of Sb_6Te_3. The first-principles calculations exhibit the characteristic surface-localized features in the narrow-gap semiconductor Sb_2Te_3 and in the gapless semimetal Sb_6Te_3, both predicted to be topologically nontrivial. Both compounds are intrinsically *p* doped, and E_F lies in the upper valence band. This hampers the acquisition of ARPES data from the TSS that are located in the bulk energy gap around the $\bar{\Gamma}$ point. A detailed analysis suggests that we actually measure a small portion of the lower part of the Dirac cone in Sb_2Te_3, and also permits discerning the spin splitting of the Rashba-split surface state located in the projected bulk gap situated around 0.8 eV below E_F [37].

To gain access to the largely unoccupied TSS, we have performed laser-based 2PPE measurements. We utilized a pump pulse with energy of 1.55 eV, smaller than the sample work function, to promote transitions into the unoccupied bands. Electron-electron scattering processes redistribute in energy the optically excited electrons on a time scale faster than the time resolution of 300 fs [38]. Subsequently, a probe pulse with an energy of 6.20 eV was used to generate photoelectrons from the transiently populated states, as sketched in Fig. 2(a). This two-photon photoemission provides a direct view of the unoccupied bands.

The 2PPE results are displayed in Figs. 2(b) for Sb_2Te_3 and 2(c) for Sb_6Te_3. They provide an unambiguous identification of the electronic states in the energy gap separating the valence band (VB) and the conduction band (CB) at the $\bar{\Gamma}$

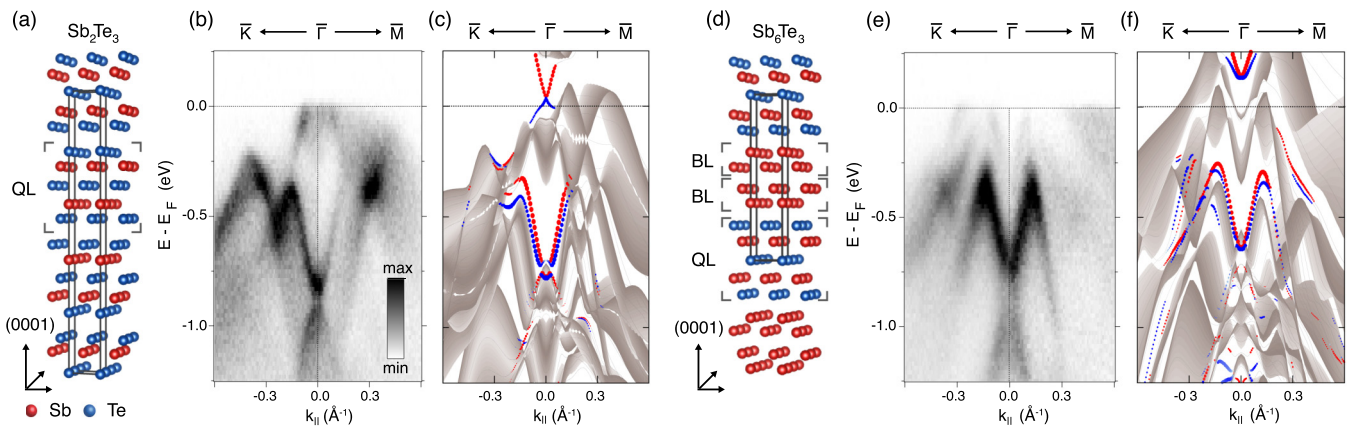

FIG. 1. (Color online) (a) Crystal structure of Sb_2Te_3 with the quintuple layer (QL) building block indicated, and (b) ARPES intensity map along the high-symmetry $\bar{\Gamma}$-$\bar{M}$ ($k_{\bar{M}} = 0.854$ Å^{-1}) and $\bar{\Gamma}$-$\bar{K}$ ($k_{\bar{K}} = 0.986$ Å^{-1}) directions of the surface Brillouin zone. Due to an intrinsic *p* doping, the Fermi level E_F lies in the bulk valence band continuum and only cuts the very bottom of the lower branch of the Dirac cone. The calculated band structure is shown in (c). The projected bulk states are shown as gray shading, and the results of the slab model are shown as lines. Red (blue) symbols indicate surface states with clockwise (counterclockwise) helicity of the in-plane spin polarization, and the size of the symbols is proportional to the surface localization. E_F has been aligned to the experimental position. (d) Crystal structure of Sb_6Te_3 with both Sb_2Te_3 QL and Sb_2 bilayer (BL) building blocks indicated. (e) ARPES intensity map from the QL-terminated surface measured along $\bar{K}$-$\bar{\Gamma}$-$\bar{M}$ ($k_{\bar{M}} = 0.849$ Å^{-1}, $k_{\bar{K}} = 0.981$ Å^{-1}). Only bulk states are visible in the heavily *p*-doped sample. The band structure is shown in (f), with the same color definitions and band alignment as in (c). The ARPES data were acquired at the ANTARES beam line with $h\nu = 70$ eV.

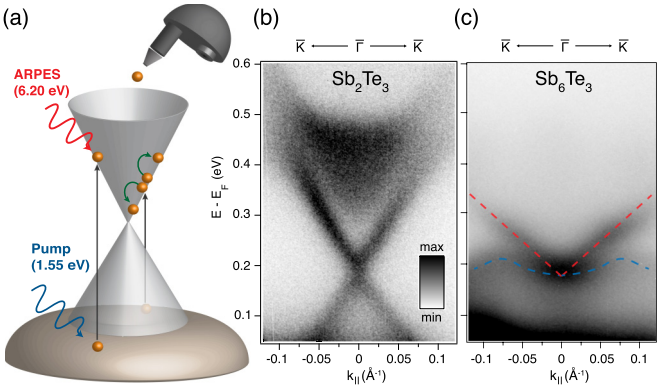

FIG. 2. (Color online) (a) Sketch of the 2PPE processes. (b) Energy-momentum 2PPE intensity map of Sb_2Te_3 along the $\bar{\Gamma}$-$\bar{K}$ direction measured at a time delay of 300 fs. The zero energy refers to the Fermi level before the arrival of the pump pulse. The corresponding map for QL-terminated Sb_6Te_3 is shown in (c), where the dashed lines tracking the dispersion of the lower and upper band are the results of fits to the data, as detailed in the Supplemental Material [37]. The data were acquired at the T-ReX Lab.

point. The bottom of the CB of Sb_2Te_3 is visible at 0.300 eV above E_F. The data show the characteristic conical dispersion of the TSS above and below the Dirac point, located at 0.180 eV above E_F. The low degree of asymmetry between the upper and lower branches of the Dirac cone implies a nearly constant band velocity $v_B = 0.38(3) \times 10^6$ m/s, consistent with previous estimates by Jiang *et al.* [25] (0.46×10^6 m/s) and Riemann *et al.* [29] (0.25×10^6 m/s). For Sb_6Te_3, the calculated band structure places the bottom of the CB at the $\bar{M}$ point, outside the window of Fig. 2(c). At variance with Sb_2Te_3, the TSS dispersion shows a large upper and lower branch asymmetry. While the upper branch disperses linearly along $\bar{\Gamma}$-$\bar{K}$ with a band velocity of $0.25(4) \times 10^6$ m/s, the lower branch dispersion is parabolic, as seen in Fig. 2(c) and discussed in more detail in the Supplemental Material [37]. This suggests that the electronic properties of the TSSs change along the superlattice series. Our first-principle calculations explain the origin of the observed difference. They show that the insertion of two Sb_2 BLs between the QLs in the unit cell of Sb_6Te_3 drives a semiconductor-to-semimetal transition, and that the resulting indirect overlap of the VB and CB forces the lower branch of the TSS band to acquire a highly nonlinear dispersion.

The evolution of the electronic structure is addressed by first-principles calculations performed on the $m = 0$–3 members of $(Sb_2)_m$-Sb_2Te_3 series, and for bulk Sb, shown in Figs. 3(a)–3(e). Our analysis reveals that the topologically nontrivial features in the band structure are remarkably robust. All investigated compositions are predicted to have a $\nu_0 = 1$ strong Z_2 invariant, resulting in an odd number of E_F crossings along the $\bar{\Gamma}$-$\bar{M}$ direction, with a large in-plane spin polarization of the TSSs. The associated Z_2 topological indices alternate between (1;000) for the even-m members and (1;111) for the odd-m members and pure Sb (see Fig. 3 and the Supplemental Material [37]). The band ordering changes along the series, resulting in the above-mentioned transition from the semiconducting phase of Sb_2Te_3 to the semimetal

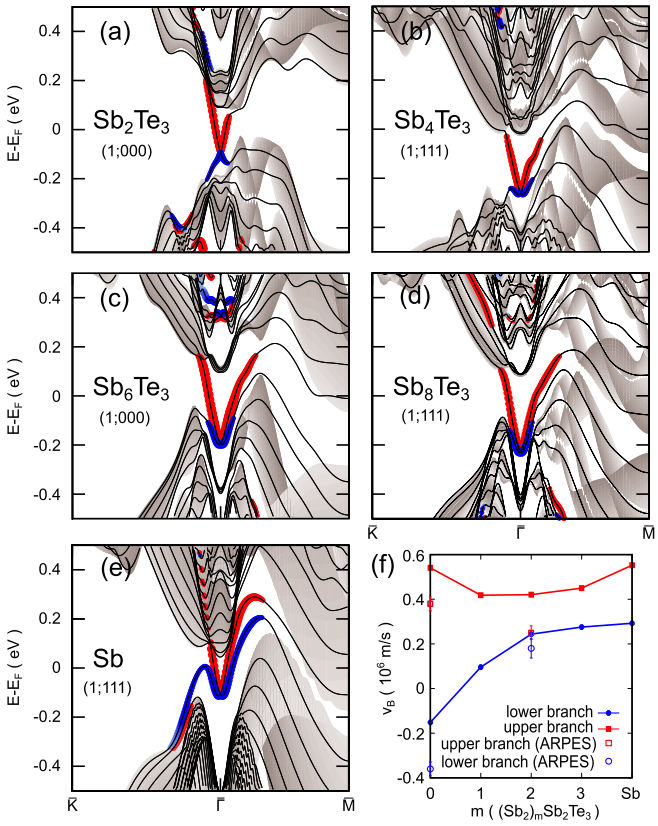

FIG. 3. (Color online) (a)–(e) Calculated electronic band structures for slab models (lines) of $(Sb_2)_m$-(Sb_2Te_3) ($m = 0$–3) and bulk Sb superimposed with the projected bulk states (gray shading). Red (blue) stands for clockwise (counterclockwise) helicity of the in-plane spin polarization. All energies are referred to the Fermi level E_F of the bulk band structure. (f) Fermi velocities for the upper (red) and lower (blue) branches of the TSS band of $(Sb_2)_m$-Sb_2Te_3 ($m = 0, 1, 2$, and 3) and Sb. The velocities were evaluated at $k_\parallel = 0.04$ Å^{-1} along the $\bar{\Gamma}$-$\bar{K}$ direction. Solid squares correspond to the calculated values whereas open squares with error bars represent the experimental values.

phase with negative indirect band gap characteristic for Sb. This transition takes place already at $m = 1$ and is driven by an elevation of the VB maximum along the $\bar{\Gamma}$-$\bar{M}$ direction that eventually overlaps in energy with the CB minimum.

The topological nature of the TSSs necessitates that the lower and upper branches of the TSS band connect to the VB and CB, respectively. In consequence, as the content of Sb increases, i.e., m gets bigger, the band dispersion of the lower branch of the TSS evolves from Dirac-like in Sb_2Te_3 to Rashba-like with a strong upper and lower branch asymmetry in the Sb-rich compounds. The band velocity serves as a proxy for this evolution. In fact, while the band velocity of the upper branch remains positive and rather constant through the entire series, the value for the velocity of the lower branch increases monotonically and changes sign from -0.15 to 0.3×10^6 m/s along the series, as seen in Fig. 3(f). This result demonstrates that a control over the electronic dispersion can be achieved in this naturally occurring series of topological superlattices, suggesting an alternative route to engineer these important states. Notice also that the exact position of the Dirac point depends on the details of the surface termination, as discussed

further in the Supplemental Material [37]. This possibly explains the observed discrepancy between experimental and calculated values of the Fermi velocities.

In all investigated materials, the TSSs show qualitatively the same spin texture. The in-plane spin polarization has clockwise spin helicity in the upper branch and counterclockwise spin helicity in the lower branch of the TSS cone. The degree of spin polarization is fairly constant over the whole energy range of the upper branch with a value of $\approx$0.6. This seems to be a common feature of all layered bismuth and antimony chalcogenide TIs [39]. By contrast, the out-of-plane spin polarization, which is related to the hexagonal warping of the TSS [40], is strongly energy dependent. In the vicinity of the Dirac point, where the TSS is isotropic, the out-of-plane spin component is close to zero. At higher energies, where the constant-energy contours are significantly warped, it increases up to 0.35 (0.43) in Sb_2Te_3 (Sb_6Te_3) at $E = 0.25$ eV above the Dirac point. The out-of-plane spin polarization is zero along the $\bar{\Gamma}$-$\bar{M}$ directions by symmetry. The quantitative details of the TSS spin texture and hexagonal warping are presented in the Supplemental Material [37].

To summarize, we investigated the occupied and unoccupied electronic states in the infinitely adaptive superlattice series $(Sb_2)_m$-Sb_2Te_3 by means of photoemission spectroscopy experiments and first-principles calculations. The results show that the topological nature of these materials and the spin texture of the topological surface states persist along the series. Remarkably, we find that by changing the chemical composition the surface-state band dispersion can be considerably modified from linear (Dirac-like) to parabolic (Rashba-like). Therefore these materials provide an exciting avenue to engineer the topological states, which is a crucial requisite for realizing different quantum phenomena and spintronics applications. In perspective, further ultrafast ARPES experiments [41–45], possibly with spin resolution, are needed to investigate the dynamics of the topological states, information of fundamental interest with important practical implications. From a methodological standpoint, the combination of ARPES and 2PPE measurements is a promising tool to explore the critical (un)occupied states in other materials.

We thank C. Tournier-Colletta for helpful discussions. We gratefully acknowledge financial support from the Swiss NSF (Grants No. 200020_149651 and No. PP00P2_133552), NCCR-MARVEL, the ERC Starting grant "TopoMat" (Grant No. 306504), and the FERMI project of Elettra-Sincrotrone and the Italian Ministry of University and Research (Grants No. FIRBRBAP045JF2 and No. FIRB-RBAP06AWK3). First-principles calculations have been performed at the Swiss National Supercomputing Centre (CSCS) under project s515.

J.C.J., G.A., and A.C. contributed equally to this work.

[1] L. Fu and C. L. Kane, Phys. Rev. B **76**, 045302 (2007).
[2] M. Z. Hasan and C. L. Kane, Rev. Mod. Phys. **82**, 3045 (2010).
[3] J. E. Moore, Nature (London) **464**, 194 (2010).
[4] D. Hsieh, Y. Xia, L. Wray, D. Qian, A. Pal, J. H. Dil, J. Osterwalder, F. Meier, G. Bihlmayer, C. L. Kane, Y. S. Hor, R. J. Cava, and M. Z. Hasan, Science **323**, 919 (2009).
[5] P. Roushan, J. Seo, C. V. Parker, Y. S. Hor, D. Hsieh, D. Qian, A. Richardella, M. Z. Hasan, R. J. Cava, and A. Yazdani, Nature (London) **460**, 1106 (2009).
[6] J. Seo, P. Roushan, H. Beidenkopf, Y. S. Hor, R. J. Cava, and A. Yazdani, Nature (London) **466**, 343 (2010).
[7] L. Fu and C. L. Kane, Phys. Rev. Lett. **100**, 096407 (2008).
[8] J. Linder, Y. Tanaka, T. Yokoyama, A. Sudbø, and N. Nagaosa, Phys. Rev. Lett. **104**, 067001 (2010).
[9] C. Seibel, H. Maaß, M. Ohtaka, S. Fiedler, C. Jünger, C.-H. Min, H. Bentmann, K. Sakamoto, and F. Reinert, Phys. Rev. B **86**, 161105 (2012).
[10] M. Bianchi, R. C. Hatch, Z. Li, P. Hofmann, F. Song, J. Mi, B. B. Iversen, Z. M. Abd El-Fattah, P. Löptien, L. Zhou, A. A. Khajetoorians, J. Wiebe, R. Wiesendanger, and J. W. Wells, ACS Nano **6**, 7009 (2012).
[11] Z. Ren, A. A. Taskin, S. Sasaki, K. Segawa, and Y. Ando, Phys. Rev. B **84**, 075316 (2011).
[12] Y. L. Chen, J. G. Analytis, J. H. Chu, Z. K. Liu, S. K. Mo, X. L. Qi, H. J. Zhang, D. H. Lu, X. Dai, Z. Fang, S. C. Zhang, I. R. Fisher, Z. Hussain, and Z. X. Shen, Science **325**, 178 (2009).
[13] T. Valla, Z.-H. Pan, D. Gardner, Y. S. Lee, and S. Chu, Phys. Rev. Lett. **108**, 117601 (2012).
[14] A. A. Burkov and L. Balents, Phys. Rev. Lett. **107**, 127205 (2011).
[15] H. Jin, J. Im, J.-H. Song, and A. J. Freeman, Phys. Rev. B **85**, 045307 (2012).
[16] K. Nakayama, K. Eto, Y. Tanaka, T. Sato, S. Souma, T. Takahashi, K. Segawa, and Y. Ando, Phys. Rev. Lett. **109**, 236804 (2012).
[17] J. W. G. Bos, H. W. Zandbergen, M.-H. Lee, N. P. Ong, and R. J. Cava, Phys. Rev. B **75**, 195203 (2007).
[18] H. Lind, S. Lidin, and U. Häussermann, Phys. Rev. B **72**, 184101 (2005).
[19] K. Kifune, Y. Kubota, T. Matsunaga, and N. Yamada, Acta Crystallogr., Sect. B: Struct. Sci. **61**, 492 (2005).
[20] J. Anderson, J. Chem. Soc. Dalton Trans., 1107 (1973).
[21] D. Hsieh, D. Qian, L. Wray, Y. Xia, Y. S. Hor, R. J. Cava, and M. Z. Hasan, Nature (London) **452**, 970 (2008).
[22] T. Kadono, K. Miyamoto, R. Nishimura, K. Kanomaru, S. Qiao, K. Shimada, H. Namatame, A. Kimura, and M. Taniguchi, Appl. Phys. Lett. **93**, 252107 (2008).
[23] H. Zhang, C.-X. Liu, X.-L. Qi, X. Dai, Z. Fang, and S.-C. Zhang, Nat. Phys. **5**, 438 (2009).
[24] Y. Xia, D. Qian, D. Hsieh, L. Wray, A. Pal, H. Lin, A. Bansil, D. Grauer, Y. S. Hor, R. J. Cava, and M. Z. Hasan, Nat. Phys. **5**, 398 (2009).
[25] Y. Jiang, Y. Wang, M. Chen, Z. Li, C. Song, K. He, L. Wang, X. Chen, X. Ma, and Q.-K. Xue, Phys. Rev. Lett. **108**, 016401 (2012).
[26] J. C. Y. Teo, L. Fu, and C. L. Kane, Phys. Rev. B **78**, 045426 (2008).

[27] M. Bianchi, D. Guan, A. Stróżecka, C. H. Voetmann, S. Bao, J. I. Pascual, A. Eiguren, and P. Hofmann, Phys. Rev. B **85**, 155431 (2012).

[28] C. Pauly, G. Bihlmayer, M. Liebmann, M. Grob, A. Georgi, D. Subramaniam, M. R. Scholz, J. Sánchez-Barriga, A. Varykhalov, S. Blügel, O. Rader, and M. Morgenstern, Phys. Rev. B **86**, 235106 (2012).

[29] J. Reimann, J. Güdde, K. Kuroda, E. V. Chulkov, and U. Höfer, Phys. Rev. B **90**, 081106 (2014).

[30] C. Seibel, H. Bentmann, J. Braun, J. Minár, H. Maaß, K. Sakamoto, M. Arita, K. Shimada, H. Ebert, and F. Reinert, Phys. Rev. Lett. **114**, 066802 (2015).

[31] J. A. Sobota *et al.*, Phys. Rev. Lett. **111**, 136802 (2013).

[32] S. D. Stolwijk, A. B. Schmidt, M. Donath, K. Sakamoto, and P. Krüger, Phys. Rev. Lett. **111**, 176402 (2013).

[33] P. Giannozzi *et al.*, J. Phys.: Condens. Matter **21**, 395502 (2009).

[34] A. Dal Corso and A. Mosca Conte, Phys. Rev. B **71**, 115106 (2005).

[35] T. L. Anderson and H. B. Krause, Acta Crystallogr., Sect. B: Struct. Sci. **30**, 1307 (1974).

[36] V. Agafonov, N. Rodier, R. Céolin, R. Bellissent, C. Bergman, and J. P. Gaspard, Acta Crystallogr., Sect. C: Cryst. Struct. Commun. **47**, 1141 (1991).

[37] See Supplemental Material at http://link.aps.org/supplemental/10.1103/PhysRevB.91.201101 for the discussion of surface terminations, measured band dispersions and further details of calculations.

[38] G. F. Giuliani and G. Vignale, *Quantum Theory of the Electron Liquid* (Cambridge University Press, Cambridge, UK, 2005).

[39] O. V. Yazyev, J. E. Moore, and S. G. Louie, Phys. Rev. Lett. **105**, 266806 (2010).

[40] L. Fu, Phys. Rev. Lett. **103**, 266801 (2009).

[41] J. A. Sobota, S. Yang, J. G. Analytis, Y. L. Chen, I. R. Fisher, P. S. Kirchmann, and Z.-X. Shen, Phys. Rev. Lett. **108**, 117403 (2012).

[42] A. Crepaldi, B. Ressel, F. Cilento, M. Zacchigna, C. Grazioli, H. Berger, P. Bugnon, K. Kern, M. Grioni, and F. Parmigiani, Phys. Rev. B **86**, 205133 (2012).

[43] J. C. Johannsen, S. Ulstrup, F. Cilento, A. Crepaldi, M. Zacchigna, C. Cacho, I. C. E. Turcu, E. Springate, F. Fromm, C. Raidel, T. Seyller, F. Parmigiani, M. Grioni, and P. Hofmann, Phys. Rev. Lett. **111**, 027403 (2013).

[44] I. Gierz, J. C. Petersen, M. Mitrano, C. Cacho, I. C. E. Turcu, E. Springate, A. Stöhr, A. Köhler, U. Starke, and A. Cavalleri, Nat. Mater. **12**, 1119 (2013).

[45] M. Hajlaoui, E. Papalazarou, J. Mauchain, L. Perfetti, A. Taleb-Ibrahimi, F. Navarin, M. Monteverde, P. Auban-Senzier, C. R. Pasquier, N. Moisan, D. Boschetto, M. Neupane, M. Z. Hasan, T. Durakiewicz, Z. Jiang, Y. Xu, I. Miotkowski, Y. P. Chen, S. Jia, H. W. Ji, R. J. Cava, and M. Marsi, Nat. Commun. **5**, 3003 (2014).